Crisis-induced Vibrational Resonance in a Phase-modulated Periodic Structure

P. O. Adesina*
Department of Physical Sciences, Redeemer's University, Ede, Nigeria and
Department of Physics, University of Ibadan, Ibadan, Nigeria

U. E. Vincent†
Department of Physical Sciences, Redeemer's University, Ede, Nigeria and
Department of Physics, Lancaster University, Lancaster LA1 4YB, United Kingdom

T. O. Roy-Layinde
Department of Physics, Olabisi Onabanjo University, Ago-Iwoye, Nigeria

O. T. Kolebaje
Department of Physics, Adeyemi Federal University of Education, Ondo, 350106 Nigeria

P. V. E. McClintock
Department of Physics, Lancaster University, Lancaster LA1 4YB, United Kingdom
(Dated: September 13, 2024)

Double vibrational resonance is reported for a driven oscillator in a periodic structure of the Josephson junction type with high-frequency phase modulation. We identify two distinct phase modulation effects, namely, resonant induction and resonant amplification, leading to the appearance of a double resonance. We analyse these vibrational resonance phenomenon theoretically and numerically, and we show that the origin of the induced resonance is traceable to a transition from periodicity to quasiperiodicity associated with an attractor-merging crisis.

Keywords: Attractor merging, Quasiperiodicity, Phase Modulation, Josephson junction, bichromatic signal

I. INTRODUCTION

Interest in nonlinear dynamical systems is motivated in part by their numerous scientific, engineering, medical and other applications. These stem from their broad range of dynamical behaviours, which are profoundly different from those of linear systems. Amongst a range of complex features, transitions associated with dynamical *crises* are of particular interest. Crises are sudden qualitative changes in a system's dynamics as a parameter is being varied, producing sudden transitions in the system's features that impact significantly on its overall evolution [1]. Four main types of crisis have been observed: attractor-merging crises [2]; boundary crises [3]; interior crises [4]; and tangent bifurcation [5] or fold crises [6]. Each of these routes represent a different mechanism by which a system can undergo a transition from one behaviour to another. In general, it is the nature of the bifurcation and phase space structure that determines the type of crisis. For instance, when two or more attractors merge to form a single attractor as a critical parameter value is exceeded, this is an example of an *attractor-merging crisis* [7, 8].

We report below a double vibrational resonance (DVR) induced by an attractor-merging crisis in a phase-modulated potential structure. Earlier studies had reported DVR induced by a number of other mechanisms, such as double symmetry breaking (sb-sb) bifurcations [9], cooperation between the time-scale separations of astrocytes, neurons, and driving signals [10], a shift in phase-locking mode [11], multiple period-doubling bifurcations of attractors [12, 13], and Hopf bifurcations [14], just to mention a few. In contrast, we consider here the onset of DVR induced by the phase-modulation of a potential. This is unlike the other system configurations such as time-delay feedback [15, 16], small disturbances, damping inhomogeneity, potential deformation, and position-dependent mass (PDM) that have also been reported to have induced DVR [11, 12, 14, 17–20].

The study of vibrational resonance (VR) originated from the work of Landa and McClintock [21] who studied a system subjected to both high and low frequency periodic forces, simultaneously, in the absence of noise. The emergence of VR has elucidated many complex features of dual-frequency-driven nonlinear systems and has enriched our understanding of their dynamical behaviours [20, 22–25]. Landa and McClintock [21] proposed this idea by replacing the role of noise in stochastic resonance (SR) with a fast periodic force. VR and SR have been found to be potentially useful in a wide variety of applications, including bulk material processing, signal processing, optical communication systems, image processing, logic gate operations, energy harvesting, and bearing-fault detection in machinery [25, 26].

Investigations of VR have been based on a number of different model configurations and approaches.

* po.adesina@ui.edu.ng
† Corresponding author:u.vincent@lancaster.ac.uk

These have included variable-mass systems [13], nonlinear damped systems [14], parametric modulated systems [27], amplitude modulation of the external periodic force [28–32] as well as frequency modulation [31]. Phase modulation of a potential plays important roles in the generation of short laser pulses in plasma channels [33], in vibrational modes of trapped ions [34], in ultrafast transmission of electrons [35] and in the creation of ultrashort light pulses [35–37]. Phase modulation based on liquid crystal spatial light modulators (LC-SLMs) has been utilized in optical tweezers, neurology and astronomy, amongst the several applications enumerated in [38]. Kenfack and Dandogbessi [39] demonstrated that modulated phase assisted by a combination of an external periodic excitation and a constant bias force, induced so-called absolute negative mobility [39]. Very recently, a time-periodic potential was shown to influence the transmission probability and conductance of an MoS_2-based circuit [40, 41]. Earlier, both random phase and periodic phase were employed in controlling chaos by either driving it from a chaotic regime to a periodic regime or *vice versa*, depending on the tuning of the phase parameters [42–45]. Notably, VR has been studied in the framework of amplitude modulation and parametric modulation [27].

However, we report below the occurrence of VR in a system in which a periodic force modulates the periodic potential's phase directly, with the other force continuing to function as the external periodic drive. We focus our attention on the impact of modulating the phase of periodic-potential on the resonance features by examining, first, the zero-phase case and, secondly, the case where the phase is non-zero. We validate this way of achieving VR both theoretically and numerically, and provide evidence that the primary resonance (without modulated phase) can be substantially enhanced within a suitably chosen parameter regime, based on phase modulation of the potential. More importantly, we report the occurrence of phase-modulation-induced VR, originating from the expansion of two coexisting attractors undergoing an *attractor-merging crisis*.

The paper is organised as follows. Following this introduction, the model equation is presented in Section II. Section III provides a theoretical assessment of the system's resonance behavior using the separation of motions approach. Sec. IV presents numerical results to validate the theoretical analysis, while Sec. V draws conclusions.

II. MODEL

We consider here the dynamics of a particle in a phase-modulated periodic structure, $V(\phi, t)$ given by,

$$V(\phi, t) = V_a[1 - \cos(\phi + g_0 \cos(\Omega_0 t))], \tag{1}$$

where V_a is the depth, $\phi_0 = g_0 \cos(\Omega_0 t)$ is a time-periodic phase modulation with g_0 and Ω_0 being the amplitude and characteristic frequency, respectively. By considering all external forces, including dissipation, the corresponding Lagrange's equation of motion is given by:

$$m\ddot{\phi} + V_a \sin(\phi + g_0 \cos(\Omega_0 t)) + \delta\dot{\phi} - f_{ext} = 0, \tag{2}$$

where m is the mass of the particle, δ is the dissipation coefficient, $f_{ext} = f_D \cos(\omega_D t)$ is the external force with f_D and ω_D being its amplitude and characteristic frequency. The frequency of the linearized motion around the minimal of the potential in the absence of the modulation is denoted as ω_0. By defining the dimensionless variables: $\tilde{t} = \omega_0 t$, $\theta = \phi$, $\lambda = \delta/m\omega_0$, $\omega = \omega_D/\omega_0$, $\Omega = \Omega_0/\omega_0$, $g = g_0$, $V_0 = V_a/m\omega_0^2$, $f = f_0$, and substituting them into Eq. (2), we obtain:

$$\frac{d^2\theta}{d\tilde{t}^2} + \lambda\frac{d\theta}{d\tilde{t}} + V_0 \sin(\theta + g\cos(\Omega\tilde{t})) = f\cos(\omega\tilde{t}). \tag{3}$$

The dimensionless equation of motion for the system, after rescaling the time with the natural period of motion $\tilde{\tau} = 2\pi/\omega_0$, and renaming the variables, then becomes:

$$\ddot{\theta} + \lambda\dot{\theta} + \frac{dV(\theta, t)}{d\theta} = f\cos(\omega t), \tag{4}$$

where θ is the dimensionless angular displacement and the dimensionless potential $V(\theta, t)$ becomes,

$$V(\theta, t) = V_0[1 - \cos(\theta + \phi(t))]. \tag{5}$$

Given the form of the potential (5), it turns out that the system can be likened to a phase-modulated Josephson-junction (JJ) device [46]. Such devices have a broad range of applications in quantum-state engineering, memory solutions, on-chip temperature sensors, electrical metrology and nanowire quantum dots [47–51]. $\phi(t) = g\cos(\Omega t)$ is the high frequency (HF) modulating force. The parameters g and f represent the amplitudes of the HF and low-frequency (LF) periodic forces, respectively. V_0 is the normalized amplitude of the potential, $f\cos(\omega t)$ is the LF excitation, and $g\cos(\Omega t)$ is the HF excitation component of the bichromatic signal. $\lambda\dot{\theta}$ is the energy dissipation term, and θ is the angular displacement. In the VR setting, $\Omega \gg \omega$.

The phase modulation can rock the particle back and forth in its potential well. This is illustrated in Figure 1 for three distinct values of the phase modulation amplitude g and for two different configurations of the snapshot times t_s leading to negative (leftward) displacement [Fig. 1(a)], and to positive (rightward) displacement [Fig. 1(b)]. For $g = 0$ (solid red lines), the particle is located at the bottoms (equilibrium positions) of the potential, at positions θ_{L0} and θ_{R0}, respectively. However, when one of the control parameters of phase is switched on, i.e., $g \neq 0$ (dotted black line and dashed green line), the particle vibrates rightward or leftward at different snapshot times t_s. Thus, the phase plays a non-trivial role in the

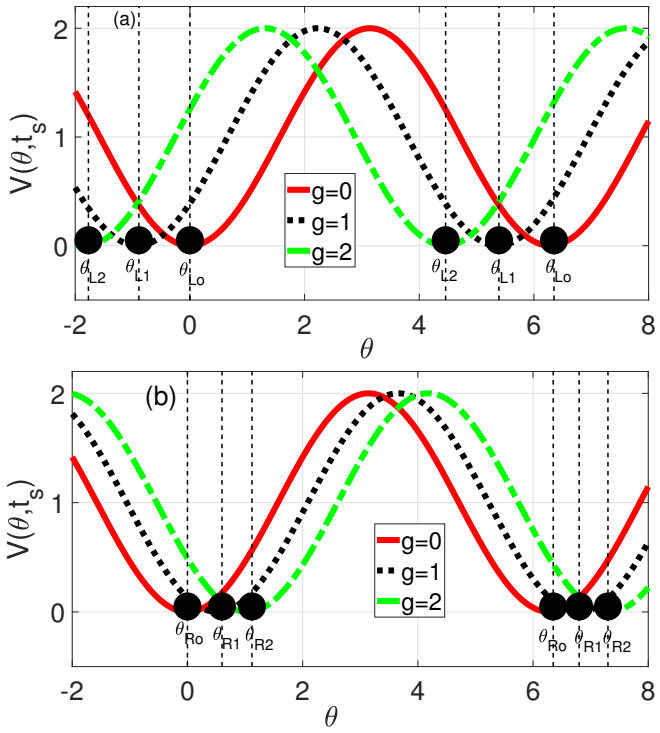

FIG. 1. [Color Online] Potential $V(\theta, t_s)$ [Eq. (5)] highlighting the effect of phase modulation with respect to the displacement θ of the particle for two snapshot times (a) $t_s = 1$ and (b) $t_s = 10$. The curves correspond to $g = 0$ (solid red lines), $g = 0.5$ (dotted black lines) and $g = 1$ (dashed green lines). The other parameters are set to $\Omega = 6.7$ and $V_0 = 1$.

action of the external LF force in rocking the particle. In the following analysis, we will obtain the effective potential and an exact expression for the particle's response as it vibrates when the phase modulation, $\phi(t)$, is switched on.

III. THEORETICAL ANALYSIS OF VR

The vibration of the particle can be analysed by separating the variables into rapid and slow motions. This leads to two differential equations. To make Eq. (4) amenable to the analysis, it will be convenient to express the potential $V(\theta, t)$ as:

$$V(\theta,t) = V_0[1 - (\cos\theta\cos(g\cos\Omega t) + \sin\theta\sin(g\cos\Omega t))]. \tag{6}$$

Thus, the system to be analyzed becomes,

$$\ddot{\theta} + \lambda\dot{\theta} + V_0[\sin(\theta)\cos(g\cos\Omega t) + \cos\theta\sin(g\cos\Omega t)] = f\cos(\omega t). \tag{7}$$

Since $\Omega \gg \omega$, the dynamics evolves on two time-scales so that the solution $\theta(t)$ of the system (7) consists of two components: (i) $\chi(t)$, which is a periodic solutions of the slowly varying oscillations whose frequency is ω, and period $2\pi/\omega$, and (ii) $\psi(t, \Omega t)$, a rapidly varying periodic oscillation with frequency Ω, fast time $\tau = \Omega t$ and period 2π. Thus,

$$\theta(t) = \chi(t) + \psi(t, \Omega t). \tag{8}$$

The average value with respect to the fast time τ, is given by

$$\overline{\psi} = \frac{1}{2\pi}\int_0^{2\pi} \psi\, d\tau = 0. \tag{9}$$

In addition, the following averages apply:

$$\begin{aligned} \overline{\cos(g\cos\Omega t)} &= J_0(g), \quad \overline{\sin(g\cos\Omega t)} = 0, \\ \overline{\sin\psi} &= \frac{1}{2\pi}\int_0^{2\pi} \sin\psi d\tau = 0, \\ \overline{\cos\psi} &= \frac{1}{2\pi}\int_0^{2\pi} \cos\psi d\tau = J_0(\psi_0), \end{aligned} \tag{10}$$

At this point, the corresponding pair of coupled differential equations for the variables χ and ψ are to be derived from the differential equation (7), with attention paid to the slow dynamics. To get the solution of the first equation, we substitute Eq (8) into Eq. (7), so that,

$$\begin{aligned} &\ddot{\chi} + \lambda\dot{\chi} + \ddot{\psi} + \lambda\dot{\psi} + V_0\sin(\chi+\psi)\cos(g\cos\Omega t) \\ &+ V_0\cos(\chi+\psi)\sin(g\cos\Omega t) \\ &= f\cos(\omega t). \end{aligned} \tag{11}$$

By taking the averages of Eq. (11) over the interval $[0, 2\pi]$, and in view of ψ being a rapidly-varying periodic function of τ, and by applying Eqs. (9) and (10), we can write:

$$\begin{aligned} &\ddot{\chi} + \lambda\dot{\chi} + V_0[\sin\chi\overline{\cos\psi} + \cos\chi\overline{\sin\psi}]\overline{\cos(g\cos\Omega t)} \\ &+ V_0[\cos\chi\overline{\cos\psi} - \sin\chi\overline{\sin\psi}]\overline{\sin(g\cos\Omega t)} \\ &= f\cos(\omega t), \end{aligned} \tag{12}$$

where ψ_0 represents the amplitude of the steady-state solution corresponding to ψ. $J_0(\psi_0)$ and $J_0(g)$ represent the zeroth-order Bessel function of the first kind. Simplifying Eq. (11) with Eq. (12) yields

$$\ddot{\chi} + \lambda\dot{\chi} + V_0[J_0(g)J_0(\psi_0)\sin\chi] = f\cos\omega t. \tag{13}$$

Equation (13) is the first of the required two coupled oscillators in the variable χ. Using Eq. (11) and the inertial approximation $\ddot{\psi} \gg \dot{\psi} \gg \psi$, where the overhead dots imply derivatives with respect to τ, we can obtain the equation for the fast oscillation ψ, reducing the resultant equation to that of a periodically-driven particle. When ψ changes rapidly, the long term periodic solution is considered in the fast time τ, i.e.,

$$\begin{aligned} &\ddot{\psi} + \lambda\dot{\psi} + V_0[\sin\chi(\cos\psi - J_0(g)J_0(\psi_0))] \\ &+ V_0\sin\psi\cos\chi\cos(g\cos\Omega t) \\ &+ V_0\cos\chi\cos\psi\sin(g\cos\Omega t) \\ &- V_0\sin\chi\sin\psi\sin(g\cos\Omega t) = 0, \end{aligned} \tag{14}$$

Under the above condition, we can free the component of the slow oscillation in Eq. (14), and consider only the cosine of the maximal value of the fast motion (i.e., $\psi = 2\pi$) for small values of g. Thus, for slow variables on the left-hand side (LHS), the 3rd term ($\sin\chi = 0$), 4th and 6th terms ($\sin\psi = 0$) all vanish. The 5th term (with $\cos\chi = 1$, and $\cos\psi = 1$) survives. For small values of g, it is clear that $\sin(g\cos\Omega t) \approx V_0 g\cos\Omega t$. The surviving term (i.e., the 5th term), reduces to $V_0\cos\chi\cos\psi\sin(g\cos\Omega t) \approx V_0 g\cos\Omega t$.

Consequently, Eq. (14) can then be reduced to:

$$\ddot{\psi} + \lambda\dot{\psi} = -G\cos\Omega t, \tag{15}$$

where $G = V_0 g$. For simplicity, $V_0 = 1$ throughout the paper, and hence $G = g$. The steady state solution of Eq. (15) is

$$\psi = \psi_0\cos(\Omega t + \phi) = \frac{-g}{\Omega\sqrt{\Omega^2+\lambda^2}}\cos(\Omega t + \phi); \tag{16}$$

$$\sin\phi = \frac{-\lambda}{\sqrt{\Omega^2+\lambda^2}}, \qquad \cos\phi = \frac{-\Omega}{\sqrt{\Omega^2+\lambda^2}}. \tag{17}$$

Assuming $\Omega \gg \lambda$, then $\psi_0 = \frac{-g}{\Omega^2}$. Thus, Eq. (13) can appropriately be written as

$$\ddot{\chi} + \lambda\dot{\chi} + V_0\left[J_0(g)J_0\left(\frac{-g}{\Omega^2}\right)\sin\chi\right] = f\cos\omega t. \tag{18}$$

Equation (18) is the required theoretical expression for the slow dynamics. It consists of the parameters of the HF signal. Eq. (18) corresponds to an effective potential:

$$V_{eff} = -V_0\left[J_0(g)J_0\left(\frac{-g}{\Omega^2}\right)\right]\cos\chi. \tag{19}$$

Figure 2 depicts the phase modulated oscillator's effective potential at different modulation amplitudes. It is evident that modulation reduces the depth of the effective potential. The oscillation occurs near $\chi = \chi_{min(max)} = 2\pi\chi$, suggesting that modulation of the phase of the potential is capable of amplifying the system's response.

At this juncture, we approximate the slow oscillation equation of (18) around the equilibrium positions $(\chi^+, \dot{\chi^+})$, where slow oscillation occurs, using the approximation $\chi^+_{\min(\max)} = 2k\pi$, where k is an integer. The oscillatory motion χ around the equilibrium can be represented in terms of its deviation from χ^+, such that $Y = \chi - \chi^+$. Thus, the equation of motion now reads:

$$\ddot{Y} + \lambda\dot{Y} + V_0 J_0(g)J_0\left(\frac{-g}{\Omega^2}\right)\sin(Y+\chi^+) = f\cos\omega t. \tag{20}$$

The points of equilibrium for the slow oscillations are $\chi^+_{\min(\max)} = 2k\pi$, where k is an integer, and $J_0(\frac{-g}{\Omega^2}).\cos\chi^+ = |J_0(\frac{-g}{\Omega^2})|$. Eq. (20) can be written as

$$\ddot{Y} + \lambda\dot{Y} + V_0|J_0(g)J_0\left(\frac{-g}{\Omega^2}\right)|\sin Y = f\cos\omega t. \tag{21}$$

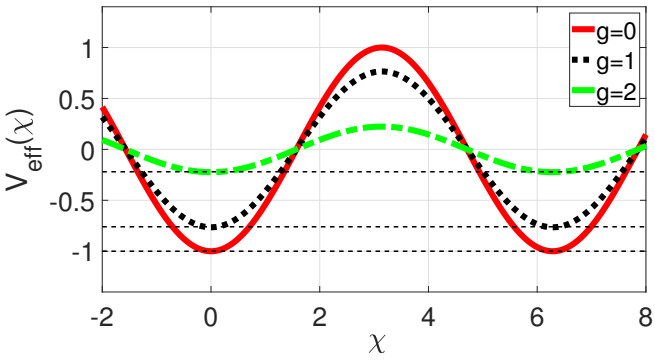

FIG. 2. [Color Online] The effective potential $V_{\rm eff}(\chi)$ given by Eq. (19), for three values of g, with $\Omega = 5$ and $V_0 = 1$

Equation (21) is the approximate analytic solution from which the amplitude of the response of the system to the HF phase modulation would be obtained.

For $f \ll 1$, $|Y| \ll 1$ and $\sin Y \approx Y$. Thus, Eq. (21) becomes

$$\ddot{Y} + \lambda\dot{Y} + \omega_r^2 Y = f\cos\omega t, \tag{22}$$

where $\omega_r = \sqrt{V_0|J_0(g)J_0(\frac{-g}{\Omega^2})|}$ represents the resonant frequency. The steady-state solution $Y(t) = A_m\cos(\omega t + \Phi)$ corresponds to Eq. (22) which gives the overall description of the system in the long time limit $t \to \infty$ with $A_m = \frac{f}{\sqrt{S}}$ and $S = \beta^2 + \lambda^2\omega^2$, and $\beta = \omega_r^2 - \omega^2$. The response amplitude is denoted by the quantity Q. It is the ratio of the amplitude of $Y(t)$, denoted by the output A_m, to the LF signal's amplitude, f:

$$Q = \frac{A_m}{f} = \frac{1}{\sqrt{(\omega_r^2-\omega^2)^2 + \lambda^2\omega^2}}. \tag{23}$$

In Eq. (23), Q is maximum when S is minimum. Thus, at resonance, the condition $\omega_r = \omega$ or $\beta = 0$, must be satisfied.

IV. NUMERICAL RESULTS

We now study the occurrence of VR numerically to investigate the result of varying the phase modulation parameter. The response was computed from the amplitudes Q_{sn} and Q_{cn} of the Fourier spectrum of the output signal, where Q_{sn} and Q_{cn} are defined by [21]:

$$Q_{sn} = \frac{2}{nT}\int_0^{nT}\theta(t)\sin\omega t\ dt \tag{24}$$
$$Q_{cn} = \frac{2}{nT}\int_0^{nT}\theta(t)\cos\omega t\ dt.$$

The system's amplitude is given by

$$A = \sqrt{Q_{sn}^2 + Q_{cn}^2}. \tag{25}$$

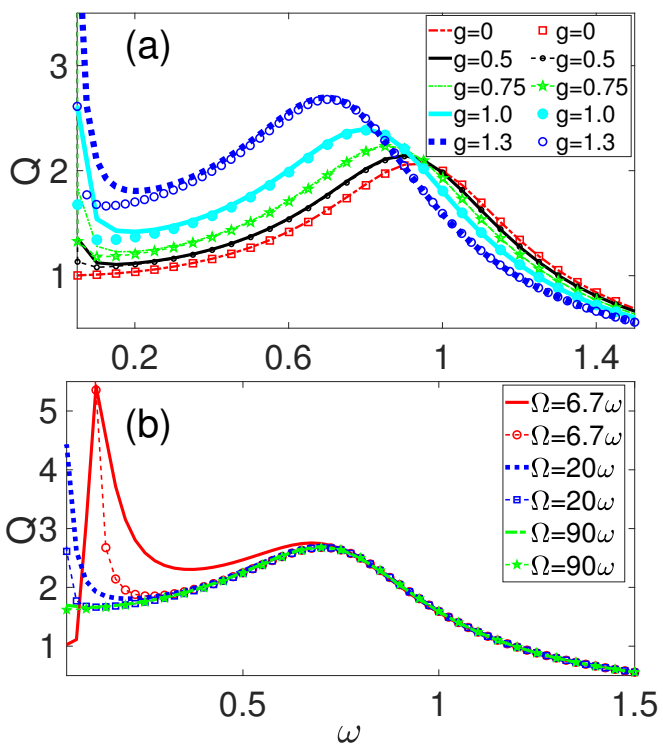

FIG. 3. [Color Online] Frequency-response curve, Q plotted as a function of ω, for (a) a fixed value of the high-frequency ($\Omega = 20\omega$) and five values of the phase modulation amplitude g, and (b) a fixed value of the phase modulation amplitude ($g = 1.3$) and three different values of the high-frequency. The various lines (solid, dashes, dots, dash-dots) represents numerically computed values of Q, while the markers show the theoretically calculated Q from Eq. (23). Other parameters are: $V_0 = 1$ and $\lambda = 0.5$.

For the LF signal, the response amplitude is given by

$$Q = \frac{A}{f} = \frac{\sqrt{Q_{sn}^2 + Q_{cn}^2}}{f}. \tag{26}$$

To compute the system's response Q, a convenient approach is to re-write Eq. (7) as two coupled first-order autonomous ordinary differential equations, i.e.,

$$\begin{aligned} \dot{\theta} &= y, \\ \dot{y} &= -\lambda\dot{\theta} - V_0 \sin\theta \cos(g\cos\Omega t) \\ &\quad -V_0 \cos\theta \sin(g\cos\Omega t) + f\cos(\omega t). \end{aligned} \tag{27}$$

We integrated Eq. (27) numerically using a fourth-order Runge-Kutta algorithm. The computation step size in the slow time t, $\Delta t = 0.01$ over a simulation time interval $T_s = nT$, with $T = \frac{2\pi}{\omega}$ being the period of the oscillation, and $n\,(= 1, 2, 3...)$ is the number of complete oscillations. Throughout the simulations, except otherwise stated, the values of the following parameters were fixed: $V_0 = 1$, $\lambda = 0.5$, $\omega = 0.75$, and $\Omega = k\omega$, where k is the frequency ratio. Zero initial conditions were used, and the relaxation time was set to $100T$. The choices made here ensured that the system is in the underdamped dynamical

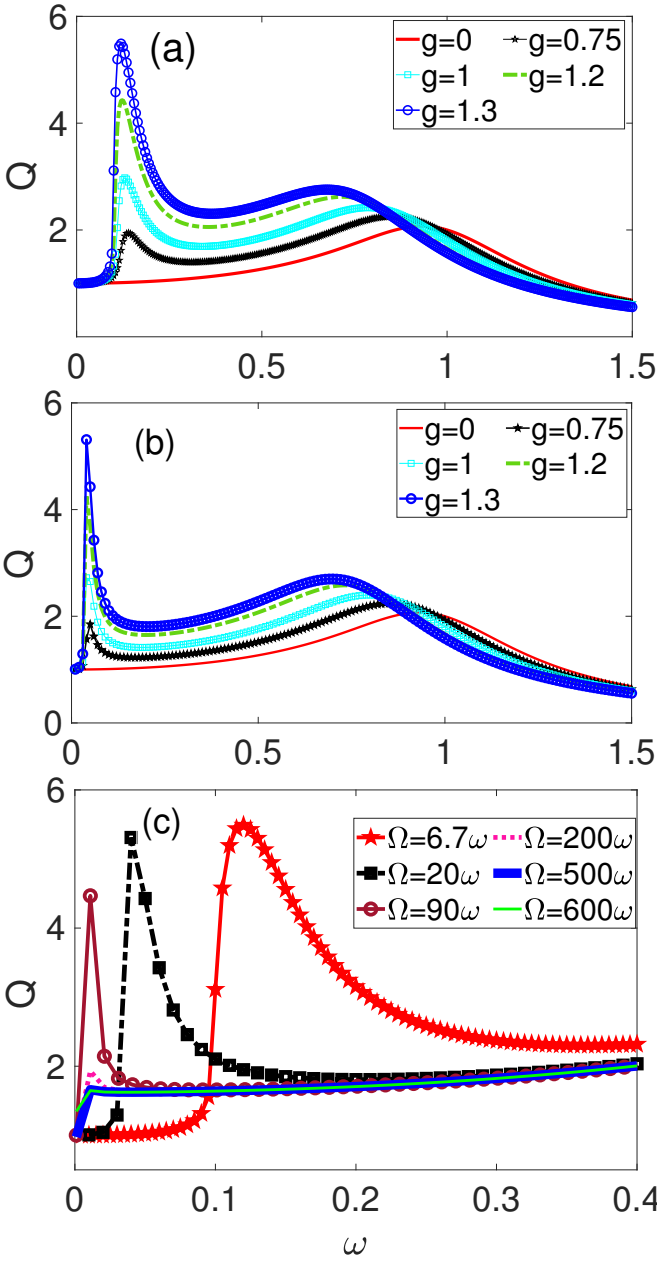

FIG. 4. [Color Online] Numerically computed frequency-response curve, with Q from Eq. (26) plotted as a function of ω for five values of the phase modulation amplitude: $g = 0$, 0.75, 1, 1.2 and 1.3. (a) $\Omega = 6.7\omega$ and (b) $\Omega = 20\omega$. In (c) g = 1.3 and Q is plotted for increasing values of Ω in the region of induced resonance.

regime, which allows for both periodic and quasiperiodic behavior.

The frequency response amplitude Q obtained analytically using Eq. (23) was compared to the response amplitude Q numerically obtained from Eq. (26). This is shown in Figure 3. Q (analytic) values are presented using different line types (solid, dash, dots, dash-dots), while Q (numerical) values are denoted by the different

markers. With the ratio $k = 20$ fixed, the plots in Figure 3(a) are for $g = 0$, 0.5, 0.75, 1.0, and 1.3 wherein VR occurs. For the lower g values (0, 0.5, and 0.75), the agreement is excellent over the entire frequency range presented, whereas, when g becomes large (e.g., $g = 1$ and $g = 1.3$), small discrepancies between the theoretical and the numerical results become evident in the very low frequency regime (typically, $\omega \lesssim 0.2$), which could be attributed to the assumptions and simplifications used for the theoretical analysis. Remarkably, the key properties of the curves, such as the trend and shape, are still in excellent agreement. Thus, the response of the system to driving forces can be predicted, albeit within some tolerance. However, in the limits when k approaches large values as demonstrated in Figure 3(b), vibrational suppression occurs in the lower frequency regime, with the theoretical predictions fitting excellently.

Figure 4(a) plots the numerically-computed frequency response Q as a function of the LF excitation frequency ω. The red curve shows the zero-phase case ($g = 0$), where a single resonance peak is evident. This primary resonance appears due to the response of the system to an LF signal in the absence of modulation. By switching on the phase modulation ($g \neq 0$), a non-trivial impact on the frequency response curve occurs, in addition to the typical VR phenomenon shown in Figure 3(a). This occurs in the frequency range $0.05 \leq \omega \leq 0.2$. For $0.5 \leq \omega \leq 1$, the response curve is strongly enhanced, whereas for $0.05 \leq \omega \leq 0.2$, resonance is induced so that, as g progressively increases, the oscillator exhibits double resonance with strong amplification.

We have investigated the range of occurrence of time-periodic phase-modulation-induced resonance, as shown in Figure 4(a), for different values of the frequency ratio k, ranging from 6.7 to 2000. We find that the phenomenon is robust, even at higher values of k, for example $6.7 \lesssim k \lesssim 600$ as illustrated in Figure 4(b) for $k = 20$. However, the LF frequency values at which the modulation-induced resonance occurs shift progressively towards lower ω values as shown in Figure 4(c), where Q is plotted for some selected Ω values, ranging from $\Omega = 6.7\omega$ to $\Omega = 600\omega$. For extremely large values of k ($k \gg 500$), the induced resonance becomes unstable and collapses to a sharp spike in the very weak LF-frequency domain, while enhancement of the primary resonance dominates. These results highlight the ability of a time-periodic phase-modulation to induce enhanced double resonance over a wide range of the LF regime. Note that double resonance has also been reported in previous works [10–12, 20]. Its occurrence has been attributed to a variety of dynamical transitions. For instance, Vincent *et al.* [12] reported DVR induced by deformation of an asymmetrical Remoissenet-Peyrard potential substrate originating from *period-doubling* bifurcations of three coexisting attractors. Roy-Layinde *et al.* [20] reported that DVR arises via cooperation between PDM parameters and nonlinear dissipation. In this latter case, the DVR was attributed to a mechanism linked

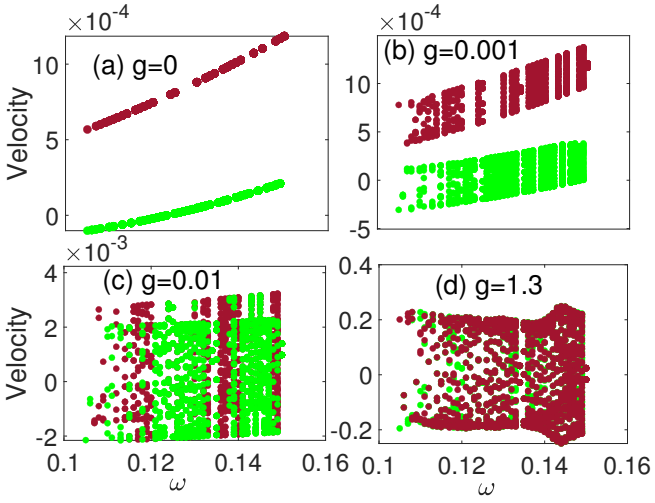

FIG. 5. [Color Online] The forward and backward bifurcation diagram of velocity, $\dot{\theta}$ as a function of ω for $g = 0$, 0.001, 0.1 and 1.3. The green points represent the forward bifurcation points, while the brown points are the backward bifurcation points. The other parameters are set as $f = 0.1$, $\lambda = 0.5$, $V_o = 1$, $\Omega = 5.025$.

to a *symmetry-breaking pitchfork bifurcation*. Variable PDM was also shown to induce DVR via multiple period-doubling bifurcations of resonant attractors in a model NH_3 molecule [13]. Here, we identify another mechanism by which DVR can be induced and enhanced: via phase modulation of the potential.

To gain insight into the appearance of DVR and uncover the hidden dynamics of our system, we explored the bifurcation of attractors, phase portrait and Poincaré section within the corresponding low-ω regime, for both zero and non-zero phase modulation of the potential of the system (4). It was evident that no resonance occurred for $g = 0$, but that it was induced when $g > 0$. In the Poincaré section, the trajectories are computed as a series of points in $(\theta, \dot{\theta})$ phase-space, with a single point per cycle of the phase modulation. That is, a point is plotted if $\omega t = \gamma + n\,2\pi$, where γ represents the phase space. Figure 5 depicts both the forward (green points) and backward (brown points) bifurcation diagrams, showing two coexisting attractor bifurcation branches. It was necessary to present both the forward and backward bifurcation structures in order to capture all the points of the two attractors, because not all values of ω have a defined velocity value in each branch. Figure 5(a) shows the bifurcation structure for the zero-phase case in which only the primary resonance exists in figure 4 for $g = 0$ for the entire ω regime: $0.5 \leq \omega \leq 1$. However, in Figure 5(b), a qualitative change in the bifurcation structure occurs when the phase-modulation is switched on by adjusting its amplitude to a very small value, $g = 0.001$. Typically, the two attractor bifurcation branches expand when the there is finite phase modulation of the potential. The expansion is progres-

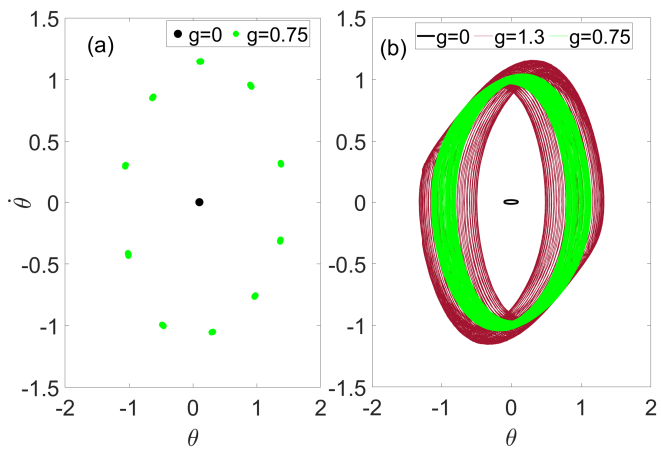

FIG. 6. [Color Online] (a)Poincaré section and (b) Phase portrait showing a transition from periodicity: ($g = 0$, black) to quasiperiodicity ($g > 0$, green), with corresponding attractor-enlargement-induced phase modulation of the potential, for increasing values from $g = 0$ t0 1.3. Other parameters are set as $f = 0.1$, $\lambda = 0.5$, $V_o = 1$, $\Omega = 5.025$.

sive with further increase in g until the two branches collide at around $g \approx 0.01$ as shown in Figure 5(c), and eventual merge. Indeed, the consequences of the progressive expansion in the attractor size, the collision, and the merger are: (i) the induction of a new resonance with fixed resonance frequency $\omega = 0.12$ for all values of g shown in Figure 5; and (ii) the amplification of the primary resonance with decreasing resonant frequency (g, ω) = [(0,0.95),(0.75,0.85),(1.0,0.8),(1.2,0.75),(1.3,0.7)]. In the ω regime where resonance is induced, the attractor expansion leads to corresponding enhancement until a maximum peak is attained at which the attractor bifurcation branches are completely merged into a single large-quasiperiodic orbit occupying nearly the entire phase space region as shown in Figure 5(d) for $g = 1.3$. Note that the velocity axis scaling in Figure 5(a-d) is different in each panel. This phenomenon is known as an *attractor-merging crisis* [52]. Figure 5(d) corresponds to the case of $g = 1.3$ in the frequency response curve of Figure 4, where the induced VR is very prominent. Thus, the attractor-merging crisis underscores the hidden dynamics by which the DVR is induced by phase modulation. Similar crisis mechanisms have been known in the past to be associated with other important dynamical phenomena, such as intermittency [53, 54], unstable dimension variability [55], multi-stability [8], spatiotemporal and transient chaos [56], flow-reversal [57] and bursting [58], to mention but a few of them.

We consolidate these results with evidence from the Poincaré and phase portrait plots. Figure 6(a) shows the Poincaré section for zero and non-zero phase modulation of the potential with $\omega = 0.1$, for the attractor located near the zero-equilibrium point. The motion of the particle is periodic for $g = 0$ (black point), but becomes an enlarged higher-order orbit, reminiscent of quasiperiodic-

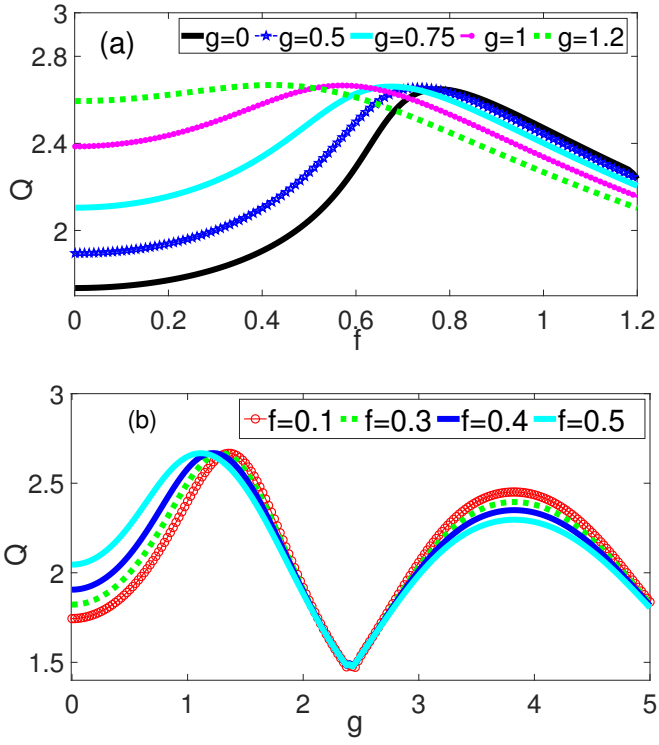

FIG. 7. [Color Online] Dependence of the response amplitude Q, computed numerically from Eq. 26: (a) on the amplitude f for five values of the phase amplitude $g = 0$, 0.5, 0.75, 1 and 1.2; and (b) on the amplitude g of the phase modulation, for $f = 0.1$, 0.3, 0.4 and 0.5.

ity, with increased amplitude of vibration when the phase modulation is activated at $g = 0.75$, (green points), implying that time-periodic phase modulation can induced antiresonance in addition to DVR. The enlarged amplitude of oscillation, as well as the transition from periodicity to quasiperiodicity, is obvious in the phase portrait shown in Figure 6(b) for both the zero-phase potential (the inner closed orbit) and the non-zero phase potential, respectively.

To complete the picture, Figure 7(a) shows the response amplitude Q with respect to the external drive's amplitude f for both the zero-phase and modulated phase scenarios. Evidently, VR occurs with enhancement of the resonance peaks as the system transitions from the zero-phase state to the phase-modulated state within the parameter range $f \in$ (0.025 to 1.2) with the peaks appearing at different values of f. Finally, Figure 7(b) shows the numerically computed response amplitude Q as a function of the amplitude g of the phase function. It is clear that resonance peaks appear as a function of g, separated by a minimum near $g = 2.3$ in each case. This feature is reminiscent of the vibrational antiresonance reported in coupled nonlinear oscillators by Sarkar and Ray [59]. The antiresonance dip at $g = 2.3$ signals the transition point at which the time-periodic modulating force switches the dynamics from weakly enhanced

VR ($0 \leq g \leq 2$) to weakly suppressed VR ($2.8 \leq g \leq 5$).

V. CONCLUSIONS

In summary, we have investigated the impact on VR of phase modulation of the potential in a periodic potential system. The contributions from this phase modulation were first identified, based on the derived effective potential. From that, we inferred that phase-modulation could be employed to amplify a weak signal in the same fashion as additive or multiplicative driving forces. We examined the frequency response curve and we found that modulating the phase of the potential can both induce and enhance resonance within certain parameter regimes, thereby leading the system to exhibit double resonance behaviour at two different frequency bandwidths. We perused the bifurcation structure in Poincaré section to gain insight into the origin of the observed double resonance, and we found two periodic attractor bifurcation branches merging to form a larger quasiperiodic orbit within the regime where DVR occurred, suggesting that it is the attractor merging crisis that underpins the induced DVR as well as the resonant amplification in the presence of the potential's phase modulation. Our theoretical results were validated numerically.

The VR phenomena investigated may have applications in periodically modulated structures such as Josephson junctions, especially in relation to superconducting electronics and quantum computing [60], and in phase-tunable thermoelectric systems [61], cryogenic memory [62], and quantum phase slips [63]. Other potential applications include optical communications [64], sound synthesis [65], and radar and sonar applications where varying the phase of broadcast and received signals allows for more precise measurement of the target's distance and velocity [66]. There are also potential applications in improving frequency-based devices such as quantum sensors [67] and one-dimensional nanostructures [68].

DATA

No new data were recorded or created in the course of this research.

FUNDING

The work was supported by the Engineering and Physical Sciences Research Council, United Kingdom (grant number EP/X004597/1)

[1] B. K. Shivamoggi, *Nonlinear Dynamics and Chaotic Phenomena: An Introduction*, Fluid Mechanics and Its Applications, Vol. 103 (Springer, 2014).
[2] Z. Hao, Q. Cao, and M. Wiercigroch, Nonlinear dynamics of the quasi-zero-stiffness SD oscillator based upon the local and global bifurcation analyses, Nonlinear Dyn. **87**, 987 (2017).
[3] L. Wang, M. Huang, W. Xu, and L. Jin, The suppression of random parameter on the boundary crisis of the smooth and discontinuous oscillator system, Nonlinear Dyn. **92**, 1147 (2018).
[4] X. Yue, W. Xu, and L. Wang, Global analysis of boundary and interior crises in an elastic impact oscillator, Commun. Nonlinear Sci. Numer. Simulat. **18**, 3567 (2013).
[5] S. Nag Chowdhury and D. Ghosh, Hidden attractors: A new chaotic system without equilibria, Eur. Phys. J. Spec. Top. **229**, 1299 (2020).
[6] K. S. Sreelatha, Dynamics of nonlinear systems: Integrable and chaotic solutions, in *Modern Perspectives in Theoretical Physics* (Springer, 2021) p. 597.
[7] U. E. Vincent and O. T. Kolebaje, Introduction to the dynamics of driven nonlinear systems, Contemp. Phys. **61**, 169 (2020).
[8] Q. Xu, Q. L. Zhang, H. Qian, H. G. Wu, and B. C. Bao, Crisis-induced coexisting multiple attractors in a second-order nonautonomous memristive diode bridge-based circuit, Int. J. Circuit Thory Appl. **46**, 1917 (2018).
[9] T. O. Roy-Layinde, J. A. Laoye, O. O. Popoola, and U. E. Vincent, Analysis of vibrational resonance in biharmonically driven plasma, Chaos **26**, 093117 (2016).
[10] A. Calim, A. Longtin, and M. Uzuntarla, Vibrational resonance in a neuron–astrocyte coupled model, Phil. Trans. Roy. Soc. A **379**, 20200267 (2021).
[11] L. Yang, W. Liu, M. Yi, C. Wang, Q. Zhu, X. Zhan, and Y. Jia, Vibrational resonance induced by transition of phase-locking modes in excitable systems, Phys. Rev. E **86**, 016209 (2012).
[12] U. E. Vincent, T. O. Roy-Layinde, O. O. Popoola, P. O. Adesina, and P. V. E. McClintock, Vibrational resonance in an oscillator with an asymmetrical deformable potential, Phys. Rev. E **98**, 062203 (2018).
[13] T. O. Roy-Layinde, K. A. Omoteso, B. A. Oyero, J. A. Laoye, and U. E. Vincent, Vibrational resonance of ammonia molecule with doubly singular position-dependent mass, Eur. Phys. J. B **95**, 80 (2022).
[14] T. O. Roy-Layinde, J. A. Laoye, O. O. Popoola, U. E. Vincent, and P. V. E. McClintock, Vibrational resonance in an inhomogeneous medium with periodic dissipation, Phys. Rev. E **96**, 032209 (2017).
[15] J. H. Yang and X. B. Liu, Delay induces quasi-periodic vibrational resonance, J. Phys. A Math. Theor **43**, 122001 (2010).
[16] D. Hu, J. Yang, and X. Liu, Delay-induced vibrational multiresonance in Fitzhugh–Nagumo system, Commun. Nonlinear Sci. Numer. Simul. **17**, 1031 (2012).
[17] Y. Yao and J. Ma, Logical stochastic and vibrational resonances induced by periodic force in the Fitzhugh–Nagumo neuron, Eur. Phys. J. Plus **137**, 1 (2022).

[18] J. H. Yang and X. B. Liu, Controlling vibrational resonance in a multistable system by time delay, Chaos **20**, 033124 (2010).

[19] S. Li, Z. Wang, J. Yang, M. A. F. Sanjuán, S. Huang, and L. Lou, Ultrasensitive vibrational resonance induced by small disturbances, Chaos **33**, 123111 (2023).

[20] T. O. Roy-Layinde, U. E. Vincent, S. A. Abolade, O. O. Popoola, J. A. Laoye, and P. V. E. McClintock, Vibrational resonances in driven oscillators with position-dependent mass, Phil. Trans. Roy. Soc. A **379**, 20200227 (2021).

[21] P. S. Landa and P. V. E. McClintock, Vibrational resonance, J. Phys. A: Math. & Gen. **33**, L433 (2000).

[22] L. Ning and K. Zhao, Vibrational resonance and bifurcation in a fractional order quintic system with distributed time delay, Phys. Scr. **97**, 055205 (2022).

[23] S. Paul and R. D. Shankar, Vibrational resonance in a driven two-level quantum system, linear and nonlinear response, Philos. Trans. Roy. Soc. A **379**, 20200231 (2021).

[24] B. I. Usama, S. Morfu, and P. Marquie, Vibrational resonance and ghost-vibrational resonance occurrence in Chua's circuit models with specific nonlinearities, Chaos Solitons Fract. **153**, 111515 (2021).

[25] J. Yang, S. Rajasekar, and M. A. Sanjuán, Vibrational resonance: A review, Phys. Rep. **1067**, 1 (2024).

[26] U. E. Vincent, P. V. E. McClintock, I. A. Khovanov, and S. Rajasekar, Vibrational and stochastic resonances in driven nonlinear systems, Phil. Trans. Roy. Soc. A **379**, 20200226 (2021).

[27] K. S. Oyeleke, O. I. Olusola, U. E. Vincent, D. Ghosh, and P. V. E. McClintock, Parametric vibrational resonance in a gyroscope driven by dual-frequency forces, Phys. Lett. A **387**, 127040 (2021).

[28] J. H. Yang and X. B. Liu, Controlling vibrational resonance in a delayed multistable system driven by an amplitude-modulated signal, Physica Scripta **82**, 035801 (2010).

[29] P. Jia, J. Yang, H. Liu, and E. Hu, Improving amplitude-modulated signals by re-scaled and twice sampling vibrational resonance methods, Pramana **91**, 1 (2018).

[30] C. Ainamon, L. A. Hinvi, F. C. Patinvoh, C. H. Miwadinou, A. V. Monwanou, and J. B. C. Orou, Influence of amplitude-modulated excitation on the dynamic behaviour of polarisation of a material, Pramana **95**, 1 (2021).

[31] V. Chinnathambi, S. Rajasekar, and M. A. F. Sanjuan, Enhanced vibrational resonance by an amplitude-modulated force, in *Recent Trends in Chaotic, Nonlinear and Complex Dynamics* (World Scientific, 2022) pp. 15–39.

[32] O. T. Kolebaje, U. E. Vincent, B. E. Benyeogor, and P. V. E. McClintock, Effect of a modulated acoustic field on the dynamics of a vibrating charged bubble, Ultrasonics **135**, 1 (2023).

[33] D. F. Gordon, B. Hafizi, R. F. Hubbard, J. R. Peñano, P. Sprangle, and A. Ting, Asymmetric self-phase modulation and compression of short laser pulses in plasma channels, Phys. Rev. Lett. **90**, 215001 (2003).

[34] X. R. Nie, C. F. Roos, and D. F. V. James, Theory of cross phase modulation for the vibrational modes of trapped ions, Phys. Lett. A **373**, 422 (2009).

[35] A. Feist, K. E. Echternkamp, J. Schauss, S. V. Yalunin, S. Schäfer, and C. Ropers, Quantum coherent optical phase modulation in an ultrafast transmission electron microscope, Nature **521**, 200 (2015).

[36] R. A. Bartels, T. C. Weinacht, N. Wagner, M. Baertschy, C. H. Greene, M. M. Murnane, and H. C. Kapteyn, Phase modulation of ultrashort light pulses using molecular rotational wave packets, Phys. Rev. Lett. **88**, 013903 (2001).

[37] D. H. White, S. K. Ruddell, and M. D. Hoogerland, Experimental realization of a quantum ratchet through phase modulation, Phys. Rev. A **88**, 063603 (2013).

[38] S. Bovetti and T. Fellin, Optical dissection of brain circuits with patterned illumination through the phase modulation of light, J. Neurosci. Methods **241**, 66 (2015).

[39] B. S. Dandogbessi and A. Kenfack, Absolute negative mobility induced by potential phase modulation, Phys. Rev. E **92**, 062903 (2015).

[40] F. Sattari and S. Mirershadi, Transport properties in a monolayer MoS_2 with time-periodic potential, Indian J. Phys. **97**, 2363 (2023).

[41] F. Sattari and S. Mirershadi, Spin-valley-dependent transport in a monolayer MoS_2 under strain and time-oscillating potential, Physica B **662**, 414975 (2023).

[42] Z. Qu, G. Hu, G. Yang, and G. Qin, Phase effect in taming nonautonomous chaos by weak harmonic perturbations, Phys. Rev. Lett. **74**, 1736 (1995).

[43] F. T. Arecchi, S. Euzzor, M. R. Gallas, J. A. C. Gallas, R. Meucci, E. Pugliese, and S. Zambrano, Exploring phase control with square pulsed perturbations, Eur. Phys. J. Spec. Top. **226**, 1785 (2017).

[44] R. Meucci, S. Euzzor, E. Pugliese, S. Zambrano, M. R. Gallas, and J. A. C. Gallas, Optimal phase-control strategy for damped-driven Duffing oscillators, Phys. Rev. Lett. **116**, 044101 (2016).

[45] Y. Lei, W. Xu, Y. Xu, and T. Fang, Chaos control by harmonic excitation with proper random phase, Chaos Solitons Fract. **21**, 1175 (2004).

[46] G. Cicogna and L. Fronzoni, Effects of parametric perturbations on the onset of chaos in the Josephson-junction model: theory and analog experiments, Phys. Rev. A **42**, 1901 (1990).

[47] Y. Makhlin, G. Schön, and A. Shnirman, Quantum-state engineering with Josephson-junction devices, Rev. Mod. Phys. **73**, 357 (2001).

[48] R. Caruso, D. Massarotti, A. Miano, V. V. Bolginov, A. B. Hamida, L. N. Karelina, G. Campagnano, I. V. Vernik, F. Tafuri, V. V. Ryazanov, *et al.*, Properties of ferromagnetic Josephson junctions for memory applications, IEEE Trans. Appl. Supercond. **28**, 1 (2018).

[49] P. Durandetto and A. Sosso, Using a Josephson junction as an effective on-chip temperature sensor, Supercond. Sci. Technol. **34**, 045008 (2021).

[50] B. Jeanneret and S. P. Benz, Application of the Josephson effect in electrical metrology, Eur. Phys. J. Spec. Top. **172**, 181 (2009).

[51] D. B. Szombati, S. Nadj-Perge, D. Car, S. R. Plissard, E. P. A. M. Bakkers, and L. P. Kouwenhoven, Josephson ϕ 0-junction in nanowire quantum dots, Nat. Phys. **12**, 568 (2016).

[52] C. Grebogi, E. Ott, and J. A. Yorke, Crises, sudden changes in chaotic attractors, and transient chaos, Physica D **7**, 181 (1983).

[53] A. L. Chian, E. L. Rempel, and C. Rogers, Crisis-induced intermittency in non-linear economic cycles, Appl. Econ. Lett. **14**, 211 (2007).

[54] C. Grebogi, E. Ott, F. Romeiras, and J. A. Yorke, Critical exponents for crisis-induced intermittency, Phys. Rev. A **36**, 5365 (1987).

[55] G. T. Kubo, R. L. Viana, S. R. Lopes, and C. Grebogi, Crisis-induced unstable dimension variability in a dynamical system, Phys Lett. A **372**, 5569 (2008).

[56] K. He, Critical behavior of crisis-induced transition to spatiotemporal chaos in parameter space, Phys. Rev. E **63**, 016218 (2000).

[57] M. Ghosh, A. Banerjee, and P. Pal, Crisis-induced flow reversals in magnetoconvection, Phys. Rev. E **104**, 015111 (2021).

[58] X. Han, C. Zhang, Y. Yu, and Q. Bi, Boundary-crisis-induced complex bursting patterns in a forced cubic map, Int. J. Bifurc. Chaos **27**, 1750051 (2017).

[59] P. Sarkar and D. S. Ray, Vibrational antiresonance in nonlinear coupled systems, Phys. Rev. E **99**, 052221 (2019).

[60] D. Zhang, Y. Chen, S. Gong, W. Wu, W. Cai, M. Ren, G. Guo, and J. Xu, All-optical modulation of quantum states by nonlinear metasurface, Light Sci. Appl. **11**, 58 (2022).

[61] G. Marchegiani, A. Braggio, and F. Giazotto, Phase-tunable thermoelectricity in a Josephson junction, Phys. Rev. Res. **2**, 043091 (2020).

[62] A. E. Madden, J. C. Willard, R. Loloee, and N. O. Birge, Phase controllable Josephson junctions for cryogenic memory, Supercond. Sci. Technol. **32**, 015001 (2018).

[63] A. E. Svetogorov, M. Taguchi, Y. Tokura, D. M. Basko, and F. W. J. Hekking, Theory of coherent quantum phase slips in josephson junction chains with periodic spatial modulations, Phys. Rev. B **97**, 104514 (2018).

[64] J. Ramón and M. Pérez, Optical phase-modulation techniques, in *Modulation in Electronics and Telecommunications*, edited by G. Dekoulis (IntechOpen, Rijeka, 2019) Chap. 5.

[65] R. Shi, N. Shen, J. Wang, W. Wang, A. Amini, N. Wang, and C. Cheng, Recent advances in fabrication strategies, phase transition modulation, and advanced applications of vanadium dioxide, Appl. Phys. Rev **6** (2019).

[66] B. Boualem, Time-frequency methods in radar, sonar, and acoustics, in *Time-Frequency Signal Analysis and Processing (Second Edition)* (Academic Press, Oxford, 2016) second edition ed., pp. 793–856.

[67] G. Wang, Y.-X. Liu, J. M. Schloss, S. T. Alsid, D. A. Braje, and P. Cappellaro, Sensing of arbitrary-frequency fields using a quantum mixer, Phys. Rev. X **12**, 021061 (2022).

[68] K. Peng and M. B. Johnston, The application of one-dimensional nanostructures in terahertz frequency devices, Appl. Phys. Rev **8**, 041314 (2021).